# GlyT1 encephalopathy: Characterization of presumably disease causing GlyT1 mutations

K. Hauf [a], L. Barsch [a,1], D. Bauer [b,1], R. Buchert [c], A. Armbruster [d], L. Frauenfeld [e], U. Grasshoff [c], V. Eulenburg [a,d,*]

[a] *Department of Anaesthesiology and Intensive Care, University of Leipzig, Leipzig, Germany*
[b] *Department of Biology, TU Darmstadt, Darmstadt, Germany*
[c] *Institute of Medical Genetics and Applied Genomics, University of Tübingen, Tübingen, Germany*
[d] *Department of Biochemistry, University of Erlangen-Nuremberg, Erlangen, Germany*
[e] *Institute of Pathology and Neuropathology, University of Tübingen, Tübingen, Germany*

## 1. Introduction

Glycine is an important inhibitory neurotransmitter predominantly in caudal regions of the central nervous system (CNS). Additionally, glycine acts as a coagonist to glutamate at N-methyl-D-aspartate receptors (NMDAR). After its presynaptic release at inhibitory synapses, it binds to glycine receptors opening an intrinsic ion channel and facilitating the chloride conductance of the postsynaptic cell (Lynch, 2004). To allow for neurotransmission to proceed with high spatial and temporal resolution, the released neurotransmitter has to be rapidly removed from the synaptic cleft and (finally) shuttled back into the presynaptic terminal. The key players that are assumed to contribute crucially to both, regulation of the extracellular glycine concentrations, as well as the efficient recycling, are the high affinity glycine transporters GlyT1 and GlyT2, which belong to the large family of *SLC6A* transporters (Gomeza et al., 2006). GlyT2 is expressed exclusively by glycinergic neurons and is responsible for the reuptake of glycine into the presynapse (Gomeza et al., 2003b). In contrast GlyT1, that is

* Corresponding author. Department of Anaesthesiology and Intensive Care, University of Leipzig, Liebigstrasse 20, 04103 Leipzig, Germany.
*E-mail address:* Volker.Eulenburg@medizin.uni-leipzig.de (V. Eulenburg).
[1] These authors contribute equally to this work.

expressed by major glial cell populations and a subset of glutamatergic neurons, facilitates the rapid glycine clearance from the synaptic cleft and additionally regulates NMDAR function by controlling the extracellular glycine concentration at a subset of excitatory synapses (Gomeza et al., 2003a; Zafra et al., 1995). Pharmacological inhibition of GlyT1 through irreversible inhibitors results in a concentration dependent elevation of the extracellular glycine level only in the CSF but not in other body fluids and without influencing other amino acid concentrations (Martina et al., 2004).

Mice lacking GlyT1 expression are not viable and die within a few hours after birth most likely due to respiratory deficiencies. Here, insufficient synaptic clearance was shown to lead to elevated extracellular glycine concentrations and thus inducing GlyR hyperactivity, which results in glycine mediated overinhibition (Gomeza et al., 2003a). This phenotype was caused by glial GlyT1 expression, since glia specific GlyT1 gene inactivation caused a phenocopy of the full GlyT1 knock out at least at neonatal stages (Eulenburg et al., 2010). In contrast inactivation of neuronal GlyT1 expression caused significant changes in the rodent behaviour suggesting altered glutamatergic signalling via NMDARs (Eulenburg et al., 2010; Martina et al., 2005).

Taken together these findings corroborate the hypothesis that the phenotype seen in GlyT1 KO mice results from overactive glycinergic inhibition caused by accumulation of glycine in the extracellular space.

Previous work suggested that mutations within the coding regions of the *SLC6A9* gene might be causal for glycine transporter 1 encephalopathy in humans (Alfadhel et al., 2016; Kurolap et al., 2016), a disease displaying many but not all facets of nonketotic hyperglycinemia, previously associated with loss of function mutations of the mitochondrial glycine cleavage system (Applegarth and Toone, 2001).

Up to now three different families with different mutations and in total 6 individuals carrying GlyT1 mutations homozygously and displaying the disease phenotype have been identified (Alfadhel et al., 2016; Kurolap et al., 2016). Symptoms described in all patients include arthrogryposis and increased nuchal translucency in ultrasound scans during pregnancy. Lifeborn infants showed severe respiratory failure requiring persistent ventilation, encephalopathy, hypotonia progressing to limp hypertonicity in response to loud sounds and tactile stimulation, global developmental delay and dysmorphic features. Further symptoms were also muscular abnormalities, including clubfeet, hyperextension of the knees and joint laxity (Alfallaj and Alfadhel, 2019). In all patients a mildly elevated glycine concentration in the CSF with no changes in serum glycine was observed, which might be a good diagnostic marker for GlyT1 encephalopathy in the future (Kurolap et al., 2016).

Three different mutations in the *SLC6A9* gene have been reported in the context of GlyT1 encephalopathy in three different families: a homozygous missense mutation c.1219 A>G (p.Ser407Gly), a homozygous small deletion c.928_932 delAAGTC (p.Lys310Phe+fs*31), and a homozygous nonsense mutation c.1717 C>T (p.Gln573*) (Alfadhel et al., 2016; Kurolap et al., 2016) due to consanguinity an autosomal recessive inheritance pattern is suggested (Alfallaj and Alfadhel, 2019).

Although the correlation of homozygous mutations and the disease phenotype suggests a direct link, the consequence of the mutation on GlyT1 functions is unclear at present. In this study we now present a functional characterization of the GlyT1 mutations found in GlyT1 encephalopathy patients including one previously unpublished mutation.

## 2. Results

A novel mutation within the *SLC6A9* gene was identified in two fetuses in subsequent pregnancies of the same parents that showed increased nuchal translucency and severe arthrogryposis in ultrasound scans. Based on these findings both pregnancies were terminated. The observed malformations were very similar to previously described cases of GlyT1 encephalopathy (Alfadhel et al., 2016; Kurolap et al., 2016). Indeed, a retrospective genomic analysis of both fetuses by NGS revealed a homozygous sequence variant at chr1:g.44010781 G>A which is localized within the predicted exon 3 of the *SLC6A9* gene encoding for GlyT1. This variant is predicted to results in an amino acid exchange from valine in position 118 to methionine (p.Val118Met, see also Table 1). Sequence comparison and a molecular model generated on basis of the crystal structure of LeuTa (Yamashita et al., 2005) suggested that this mutation is localized within the transmembrane domain (TM)1 close to the predicted substrate and ion binding site of GlyT1 (see Fig. 1A and B). Subsequently, Sanger sequencing of the relevant exon in genomic DNA from the parents showed that both of them were heterozygous carriers of the mutation (Fig. 1C). A later born healthy sibling was shown to be wild-type for the respective mutation, thus further supporting the hypothesis that the observed GlyT1 mutation is associated with the disease phenotype. To investigate the consequences of this, and of the previously identified mutations found in patients with GlyT1 encephalopathy on transporter function, we set out for a detailed *in-vitro* characterization of these mutations to determine if the phenotype seen in GlyT1 encephalopathy might correlate to a loss of function of GlyT1 protein.

The different mutations that have been identified in GlyT1 encephalopathy patients including the predicted changes on the GlyT1 protein have been summarized in Table 1. These mutations include two missense mutations, one previously identified by Alfadhel et al. (2016) that is predicted to cause an amino acid exchange at positions 407 (p.Ser407Gly), and the missense mutation first described in this study, that is predicted to cause an amino acid exchange at position 118 (p.Val118Met). Additionally, two mutations previously described by Kurolap et al. (2016) that are predicted to result in truncated transporter proteins were characterized. Moreover, a transporter carrying a SNP in position 594 (p.Gln594Glu), which did not result in a disease phenotype, was added to the characterization (Fig. 1A).

To analyse the consequences of the respective mutations on transporter function, we introduced the respective changes in an expression construct containing the cDNA sequence of human GlyT1c (R&D Systems) by site directed mutagenesis. All constructs were transfected into HEK293 cells and detergent extracts were prepared 2 days after transfection. Western blot analysis of cells expressing the respective GlyT1 mutants or the wild-type GlyT1 were probed with an antibody raised against the C-terminal domain of GlyT1. Here, in samples from wild-type GlyT1 expressing cells ($hGlyT1^{wt}$) as well as in those from cells expressing $hGlyT1^{S407G}$, $hGlyT1^{V118M}$ or the SNP $hGlyT1^{Q594E}$ showed an indistinguishable pattern of immunoreactive bands consistent with a full-length expressed glycine transporter. In Western blot analysis of the mutant $hGlyT1^{S407G}$ protein expressing cells the slight variations in band intensities observed are indicative for differences in expression levels, most likely resulting from differences in transfection efficacies (Fig. 1D). In all three samples a major band at ca. 80 kDa most likely representing the fully mature monomer and weaker bands at around 60 kDa most

**Table 1**
List of the hGlyT1 mutations characterized in this study, including reference of the first publication, its genetic description and predicted molecular weight.

| Mutation | Source | SLC6A9 | Mutation | Predicted Protein Weight |
|---|---|---|---|---|
| $hGlyT1^{S407G}$ | Alfadhel et al. (2016) | ch1:g.44001591 A>G | Point Mutant | 78.24 kDa |
| $hGlyT1^{K310F+fs*31}$ | Kurolap et al. (2016) | ch1: g.44002864–44002868 del | Frame Shift | 37.12 kDa |
| $hGlyT1^{Q573*}$ | Kurolap et al. (2016) | ch1:g.44000806 C>T | Point Mutant | 63.13 kDa |
| $hGlyT1^{V118M}$ | this study | ch1:g.44010781 G>A | Point Mutant | 78.3 kDa |
| $hGlyT1^{Q594E}$ | this study | ch1:g.43998001 G>C | Point Mutant | 78.27 kDa |

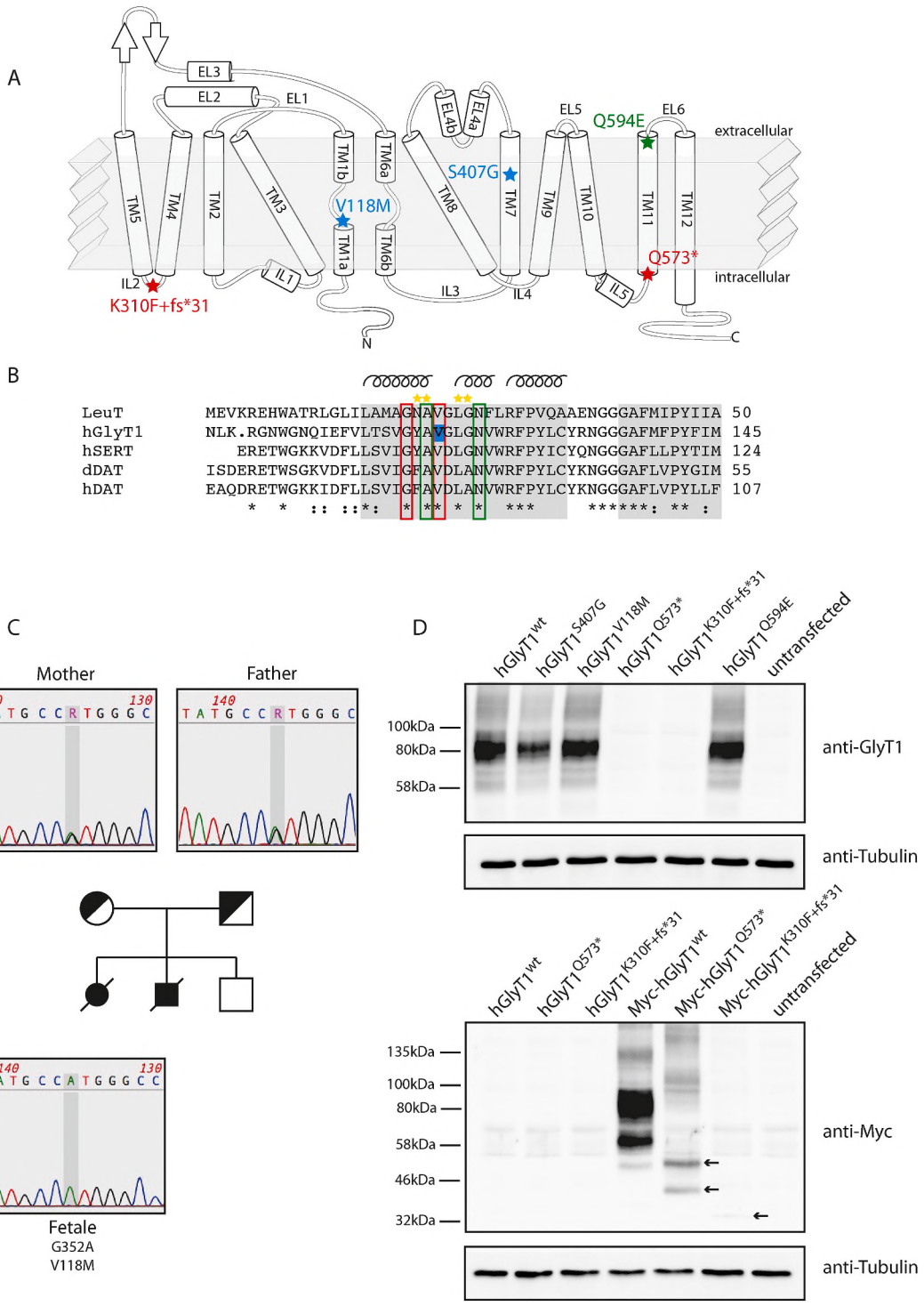


**Fig. 1.** GlyT1 encephalopathy associated GlyT1 Variants and SLC6A9 sequence analysis of a novel hGlyT1$^{V118M}$ mutation. (A) Schematic drawing of the GlyT1 membrane topology based on homology to LeuTa. Previously identified mutations found in GlyT1 encephalopathy patients as well as a novel mutation suggested to cause GlyT1 encephalopathy are indicated in TM1, 7, 11 and IL2. (B) Amino acid sequence alignment LeuTa, GlyT1 and other members of the SLC6A family. Transmembrane domains, predicted on basis of the crystal structure of LeuTa are indicated as grey boxes (Yamashita et al., 2005). Position of the novel hGlyt1 mutation V118M is coloured blue. The green and red boxes indicate residues contributing to the binding of sodium 1 and 2. Residues contributing to substrate binding in LeuTa are marked by yellow stars. Sequence alignment was calculated using Clustal Omega (Sievers et al., 2011). Amino acid identity is indicated by a (*), amino acid similarity is indicated by an (:). (C) Pedigree and sequence analysis of a novel hGlyt1$^{V118M}$ mutation identified in two fetuses showing symptoms similar to those seen in GlyT1 encephalopathy patients. Position of the mutation in the sequence analysis is indicated. (D) Western-blot analysis of HEK293 cell detergent extracts from cells expressing the indicated hGlyT1 expression constructs. Blots were probed with antibodies against the C-terminal domain of GlyT1 or the Myc-tag, as indicated. An anti-Tubulin antibody was used as a loading control.

likely representing an immature, core-glycosylated transporter monomer and a band most likely representing the dimer of the mature isoform at around 190 kDa were observed (Bartholomäus et al., 2008). For the mutations hGlyT1$^{Q573*}$ and hGlyT1$^{K310F+fs*31}$ no immune reactive bands were detected, consistent with a truncation at positions 573 and 341, respectively (Fig. 1D). To allow for a detection of these truncated proteins, a 10 amino acid long Myc (around 1 kDa) was inserted into the expression constructs for these GlyT1 mutants and wild-type GlyT1 after the first 13 amino acids of the N-terminus of GlyT1 by site directed mutagenesis. Immunoblot of detergent extracts of Myc-tagged GlyT1 (Myc-hGlyT1) transfected HEK293 cells revealed an almost identical band pattern as compared to hGlyT1 expressing cells regardless if GlyT1 or Myc specific antibodies were used for detection. Due to a higher exposition time, even the very small fraction of the presumably fully unglycosylated monomer at around 50 kDa is visible in the Myc-hGlyT1$^{wt}$ lane (Fig. 1D). In samples from Myc-hGlyT1$^{Q573*}$ expressing cells two immunreactive bands at around 40 and 50 kDa and a (double-) band at around 100 kDa, followed by a slightly smaller band at around 150 kDa were observed, which is consistent with a truncated GlyT1 transporter being expressed in these cells, that aggregates to SDS resistant dimers and higher order oligomers. The frame shift mutation hGlyT1$^{K310F+fs*31}$ shows just a faint band at around 32 kDa, consistent with a rather unstable truncated GlyT1 protein being expressed. Otherwise only faint unspecific bands are visible, that are also seen in the untransfected control lysate (Fig. 1D).

To analyse the subcellular distribution of the respective hGlyT1 mutants, HEK293 cells were transfected with the respective expression constructs and GlyT1 protein was visualized by immunohistochemistry and confocal microscopy. Here, analysis of wild-type hGlyT1 and the three apparently full length expressed mutants revealed a prevailing immunoreactivity within the plasma-membrane of the transfected cells, suggesting that the respective mutation does not interfere with membrane insertion of the transporter (Fig. 2A). In contrast, the expression of the truncating mutations hGlyT1$^{Q573*}$ and hGlyT1$^{K310F+fs*31}$ did not produce any immunoreactive signals when antibodies against the C-terminal domain of GlyT1 were used (data not shown). Similar to the wild-type hGlyT1, also the Myc-tagged full length hGlyT1 transporter was clearly localized within the plasma membrane. Here a colocalization of GlyT1 and Myc immunoreactivity was observed (Fig. 2B). After expression of the truncated Myc-tagged transporters Myc-hGlyT1$^{Q573*}$ and Myc-hGlyT1$^{K310F+fs*31}$, however, only Myc immunoreactivity was observed in intracellular compartments, colocalizing with a endoplasmatic reticulum (ER) retained DS-red, suggesting, that the truncation results in intracellular retention within the ER (Fig. 2C). To allow for a quantitative assessment of the level of surface expression of the respective mutations, each construct was cotransfected with an expression construct for wild-type mouse GlyT2, which was previously shown to efficiently localize to the plasma membrane (Armsen et al., 2007). The Mander's coefficient for the GlyT2 and GlyT1 immunoreactivity indicative for the colocalization of both immunoreactivities was determined using ImageJ (Bolte and Cordelières, 2006; Schindelin et al., 2012). Here, both, the hGlyT1$^{V118M}$ or the SNP hGlyT1$^{Q594E}$ were indistinguishable from wildtype hGlyT1, whereas the Mander's M2 Coefficient for hGlyT1$^{S407G}$, which represents the fraction of GlyT2 overlapping GlyT1 immunofluorescence was significantly reduced, whereas the M1 coefficient, representing the fraction of GlyT1 immunofluorescence overlapping with that of GlyT2, was only slightly but not significantly reduced. These findings might result from the lower expression level of hGlyT1$^{S407G}$ although a slightly reduced membrane insertion of the transporter cannot be excluded (Fig. 2D and E).

These results were corroborated by surface biotinylation experiments. Here, a major fraction of the apparent mature, fully glycosylated full length hGlyT1 protein was detected in the streptavidine-agarose bound surface fraction, representing the membrane protein fraction for both the wild-type hGlyT1 and its mutations hGlyT1$^{S407G}$, hGlyT1$^{V118M}$ and hGlyT1$^{Q594E}$. In all samples the band at ca. 60 kDa, presumably representing an immature, only core glycosylated GlyT1 protein was excluded from this fraction (Fig. 3A). Interestingly, although immunocytochemical stainings suggest an almost complete surface localization of the full length hGlyT1 proteins, only a fraction of the mature hGlyT1 was detected in the membrane protein fraction, whereas some mature GlyT1 was also observed in the presumptive intracellular unbound fraction. To investigate if these findings results from insufficient labelling and/or binding to the streptavidine agarose beads of the hGlyT1 proteins, we cotransfected the cells used for our biotinylation experiments with a GlyT2 expression plasmid. For GlyT2 previous studies have shown an almost complete enrichment of the immunreactive band at 100 kDa representing the mature GlyT2 isoform in the surface fraction of surface biotinylation experiments (Armsen et al., 2007). In our experiments performed here, however, some residual immunreactivity at 100 kDa was also observed in the unbound intracellular fraction, indicating insufficient biotinylation and/or precipitation of biotinylated proteins. This was not caused by saturation of the strepavidine beads, since increasing the bead volume did not change the precipitation efficacy. When comparing ratio of intensities of the presumably mature hGlyT1 isoforms in the different fractions of the biotinylation experiment, weaker signals within the surface fraction were observed in samples from hGlyT1$^{S407G}$ and hGlyT1$^{V118M}$ expressing cells. Additionally, however, also the immunreactive signal intensity in flow-through fractions was reduced, suggesting that this is caused by a loss of protein e.g. due to precipitation under assay conditions used, and not due to a reduced surface expression of the respective mutant (Fig. 3A).

In samples derived from HEK cell lysates expressing the truncated hGlyT1$^{Q573*}$ or hGlyT1$^{K310F+fs31}$ only a very minor fraction or no GlyT1 immunoreactive protein at all were detected in the fraction representing the membrane proteins, consistent with a predominantly intracellular localization of the respective proteins. For hGlyT1$^{Q573*}$ a small part of the ca. 100 kDa aggregates appear in the pellet fraction. Whether this is due to very low surface expression of the truncated protein or due to precipitation of the protein under the assay conditions used, is unclear at present (Fig. 3B).

It was shown previously that the posttranslational modification of the GlyTs corresponds to their surface trafficking. Here, only fully glycosylated GlyT2 was shown to reach the plasma membrane (Martínez-Maza et al., 2001). To analyse the glycosylation pattern of the respective mutant transporters, HEK cell detergent extracts from cells expressing either wild-type hGlyT1 or one of the respective mutant transporters were treated with EndoH (E), a deglycosidase that cleaves high mannose O-linked oligosaccharides from glycoproteins, and PNGaseF (P), that cleaves almost all glycans from glycoproteins (Fig. 3C and D).

In untreated and EndoH treated lysates from hGlyT1 expressing cells, the presumably mature transporter isoform at ca. 80 kDa was the most prevailing isoform, whereas PNGaseF resulted in an apparent shift of this band to ca. 50 kDa most likely representing the fully unglycosylated transporter. In samples form cells expressing the wild-type hGlyT1 protein, an EndoH sensitive band at around 60 kDa representing a core-glycosylated isoform is faintly visible. A similar pattern was also found in the lysates from cells expressing point mutants hGlyT1$^{S407G}$ and hGlyT1$^{V118M}$ and the SNP hGlyT1$^{Q594E}$, demonstrating that the post-translational modification was not disturbed by these mutations (Fig. 3C). Looking at the deglycosylation pattern of the truncated mutants hGlyT1$^{Q573*}$ only a faint band at ca. 50 kDa showed sensitivity to both Endo H and PNGaseF, suggesting a core glycosylation usually occurring in the ER, whereas no significant change in the band pattern was observed in samples from hGlyT1$^{K310F+fs*31}$ expressing cells, suggesting this mutant hGlyT1 protein was not posttranslationally glycosylated at all (Fig. 3D).

In order to investigate the impact of V118M and S407G on the molecular structure of the transporter, we performed all-atom molecular dynamics (MD) simulations using a hGlyT1 homology model generated

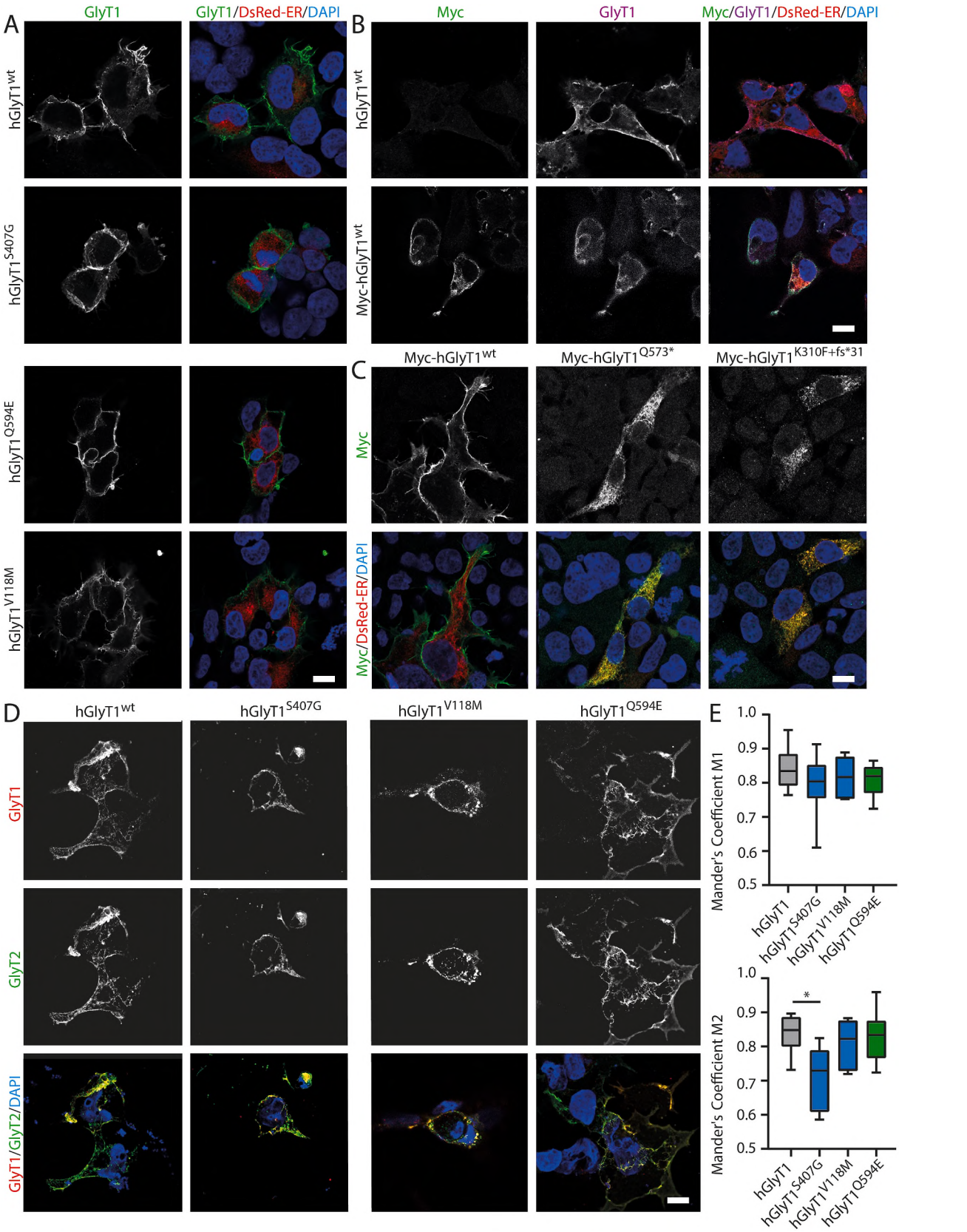


*(caption on next page)*

**Fig. 2.** Subcellular localization of hGlyT1 Mutants. (A) Immunocytochemical analysis of HEK293 cells expressing the indicated hGlyT1 expression constructs and an ER localized DS-Red (red) 48 h after transfection, using an anti-GlyT1 antibody (green) and the nuclei stained with DAPI (blue). (B) Immuncytochemical analysis of HEK293 cells expressing wild-type hGlyT1 or Myc-hGlyT1 and an ER-retained DS-Red (red) using GlyT1 (purple) and Myc (green) specific antibodies. Nuclei are visualized by DAPI (blue) staining. Note that in Myc-hGlyT1 transfected cells Myc and GlyT1 immunreactivity show a complete overlap. (C) Immuncytochemical analysis of HEK293 cells transfected with the indicated truncated Myc-hGlyT1 expression constructs and an ER retained DSRed. Nuclei were visualized by DAPI staining (blue). Myc-tagged truncated mutant hGlyT1 proteins were visualized by a Myc antibody (green). Note that Myc immunreactivity localizes to the ER as indicated by colocalization with DsRed fluorescence as indicated by yellow colour. (D) HEK293 cells coexpressing the respective hGlyT1 mutant and mGlyT2 were analysed by immunofluorescence using GlyT1 (red) and GlyT2 (green) specific antibodies. Colocalization of both fluorescences was quantified using ImageJ Mander's coefficient (E). M1 indicates the fraction of hGlyT1 overlapping mGlyT2 and M2 indicates the fraction of GlyT2 overlapping GlyT1 ($n < 6$) (Bolte and Cordelières, 2006; Schindelin et al., 2012). The scale bar indicates 10 μm.

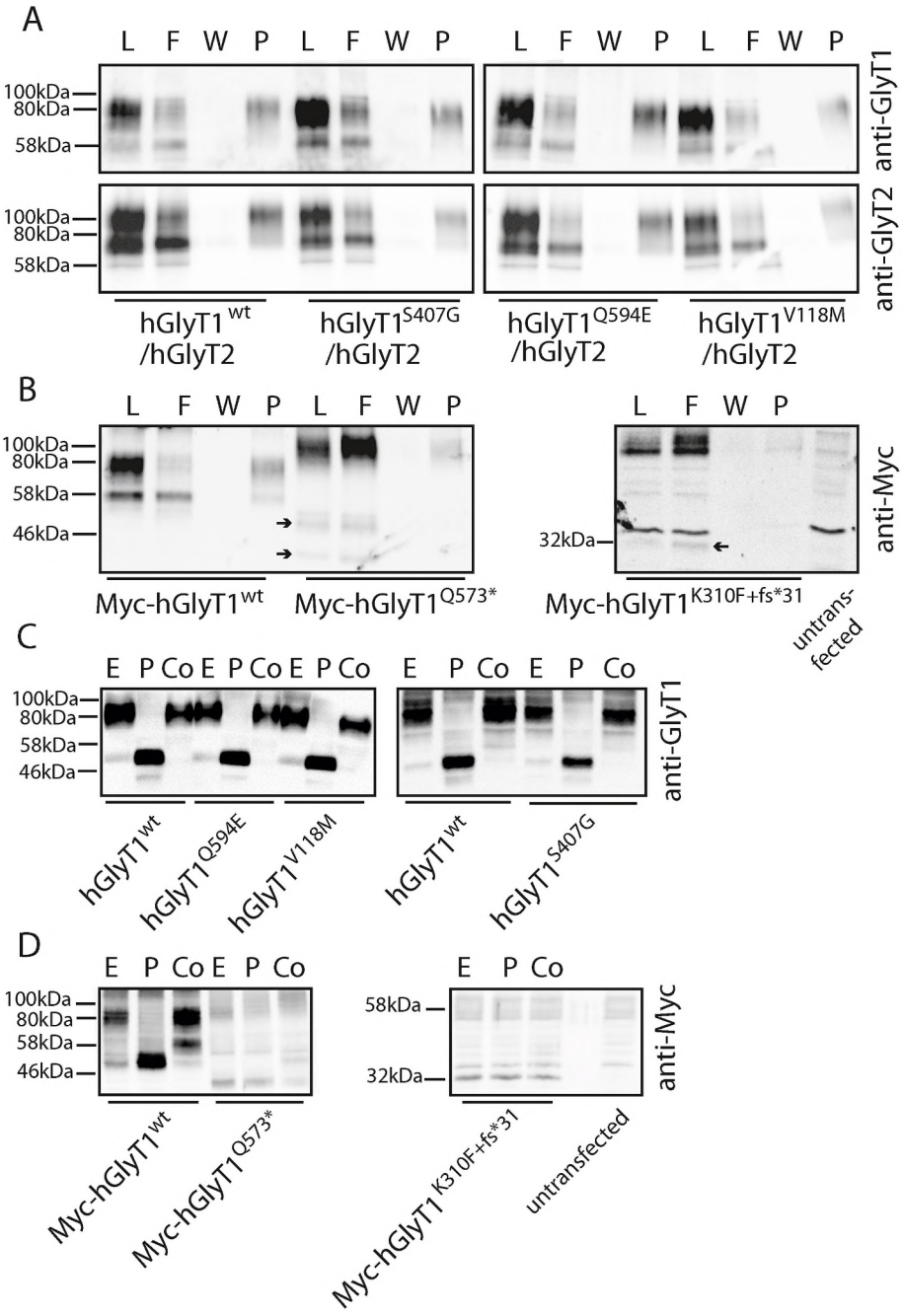


**Fig. 3.** Subcellular localization and posttranslational modification of hGlyT1 Mutations. (A) Western-Blot analysis of a surface biotinylation experiments on HEK293 cells transfected with the different full length hGlyT1 and wt-mGlyT2 expression plasmids as indicated, using an anti-GlyT1 and anti-GlyT2 antibody. The lysate (L), flow through (F), wash control (W) and pellet (P) fractions are indicated ($n = 3$). (B) Surface biotinylation experiments on HEK293 cells transfected with the indicated Myc-tagged hGlyT1 proteins using a Myc antibody for analysis. ($n > 3$). (C) Immunoblots detected with an anti-GlyT1 antibody of detergent extracts of wild-type and full-length hGlyT1 mutant expressing HEK293 cells treated with EndoH (E) and PNGaseF (P) and compared to a control without enzyme (Co) ($n > 5$). (D) Immunoblots detected with an anti Myc antibody of detergent extracts of Myc-tagged wild-type and the indicated hGlyT1 mutation expressing HEK293 cell detergent extracts treated with EndoH (E), PNGaseF (P), and compared to a control without enzyme (Co) ($n > 5$).

on basis of the LeuTa crystal structure in its wild type and mutated form with bound glycine and associated ions. The two mutations showed comparable stability and no large deviation in secondary structure compared to the $hGlyT1^{WT}$ transporter over 250 ns of simulation (Fig. 4B). This confirms experimental findings showing no significant impact on protein folding and trafficking. Representative snapshots showing the side chain orientation of $hGlyT1^{V118M}$ and $hGlyT1^{S407G}$ are depicted in Fig. 4A. We then calculated the frequency of polar contacts

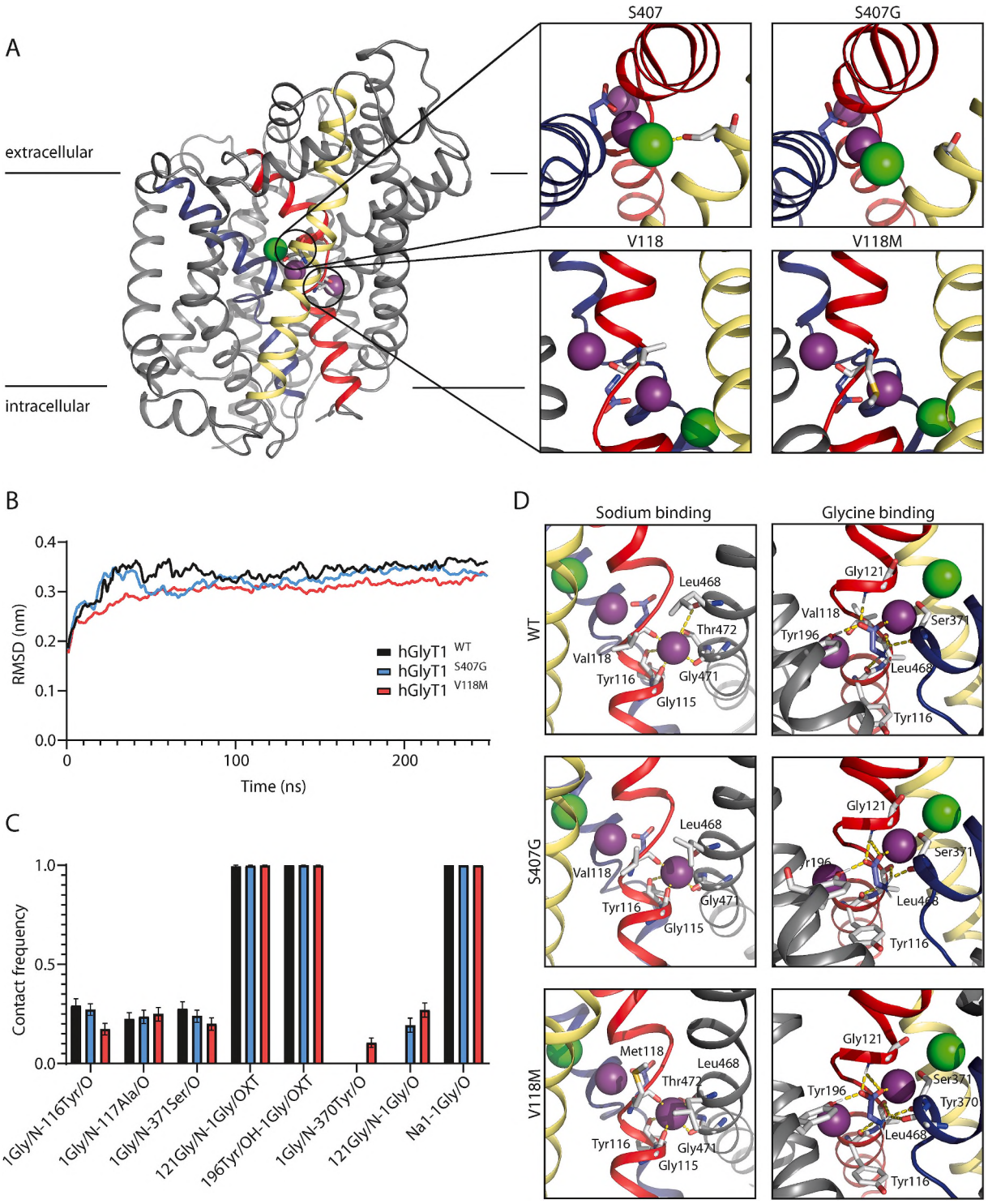


**Fig. 4.** All-atom molecular dynamics (MD) simulations using a hGlyT1 homology model in its wild type and mutated form with bound glycine and associated ions. (A) Model of hGlyT1 generated on basis of LeuTa (Bartholomäus et al., 2008) or the respective mutants. Since wild-type and mutant hGlyT1 showed almost identical overall structure only wild-type hGlyT1 is shown. Representative snapshots display the side chain orientation of the wild-type and mutants visualizing predicted molecular changes within the GlyT1 protein caused by the respective mutation. Sodium ions are indicated in purple, chloride in green, and the glycine ligand is depicted in blue. (B) Transporter stability over 250 ns of simulation indicated by backbone root-mean-squared deviation (RMSD). (C) Frequency of polar contacts responsible for stabilizing the glycine ligand in its bound form during the dynamic simulation. (D) Representative snapshots of sodium and ligand binding in wild type and mutant hGlyT1.

responsible for stabilizing the glycine ligand in its bound form (Fig. 4C and D). While S407G has no significant effect on ligand binding, V118M leads to slightly reduced hydrogen bonding and altered binding patterns for residues that stabilize the ligand aminogroup natively (i.e. contacts involving residues Y116 and S371).

For the functional analysis of the hGlyT1 mutations, the different constructs were expressed in *Xenopus laevis* oocytes and transport associated currents were analysed by two-electrode voltage clamp (TEVC)

recordings. Here, glycine induced currents were readily detected from oocytes expressing either hGlyT1$^{wt}$, GlyT1$^{Q594E}$, hGlyT1$^{S407G}$ or hGlyT1$^{V118M}$. Current maximal amplitudes, however, appeared significantly smaller in oocytes expressing the last two constructs (hGlyT1$^{S407G}$ 64.5 nA ± 16 nA (n = 10); hGlyT1$^{V118M}$ 15.2 nA ± 5.0 nA (n = 15) in contrast to hGlyT1$^{wt}$ 106.1 nA ± 27.2 nA (n = 15) and GlyT1$^{Q594E}$ 133.2 nA ± 44.9 nA (n = 12) expressing oocytes; Fig. 5A). Virtually no glycine induced currents were observed in oocytes expressing hGlyT1$^{Q573}$* and hGlyT1$^{K310F+fs*31}$, demonstrating that these transporter mutants do not show any (residual) transport activity. This is in line with the previous results, indicating that they are not processed correctly and retained intracellularly. Subsequently, the affinity for the substrate glycine was determined. Here, the hGlyT1$^{wt}$ revealed a $K_m$ of 11 μM (95% CI 11.0–12.6 μM, n = 16). For the SNP hGlyT1$^{Q594E}$ a $K_m$ of 18 μM (95% CI 17–19 μM, n = 13) was established that was very similar to that determined on hGlyT1$^{wt}$ expressing oocytes. For the hGlyT1$^{S407G}$ mutant a $K_m$ value of 514 μM (95% CI 438–602 μM, n = 10) was calculated, demonstrating that this mutation results in a more than 50 times reduction in glycine affinity compared to that determined for hGlyT1$^{wt}$. A similarly reduced affinity for glycine was determined for the hGlyT1$^{V118M}$ mutation that showed a Km of 373 μM (n = 15; 95% CI 320–436 μM; Fig. 5B). Taken together these data demonstrate that all mutations found in GlyT1 encephalopathy patients resulted in a severe impairment of GlyT1 function that is predicted to result in a complete loss of GlyT1 mediated glycine transport activity *in-vivo*.

## 3. Discussion

In this study, we show that all hGlyT1 mutations previously identified in patients with GlyT1 encephalopathy, as well as a novel mutation identified in two fetuses with abnormalities consistent with GlyT1 encephalopathy, result in severe transporter dysfunction. These findings support the hypothesis that the identified GlyT1 mutations are causative for the phenotype of GlyT1 encephalopathy. The GlyT1 mutations, hGlyT1$^{Q573}$* and hGlyT1$^{K310F+fs*31}$ identified by Kurolap et al. (2016) have been predicted to be truncating mutations. In hGlyT1$^{Q573}$* a stop codon before TM11 is predicted to result in a transporter lacking TM11 and TM12. hGlyT1$^{K310F+fs*31}$ is predicted to cause a frame shift at position 310 resulting in a premature stop codon and a truncation of the transporter after TM4. Here, consistent with previous findings e.g. on mutations of GlyT2 found in hyperekplexia patients, the truncation of the transporter resulted in an ER retained incompletely processed

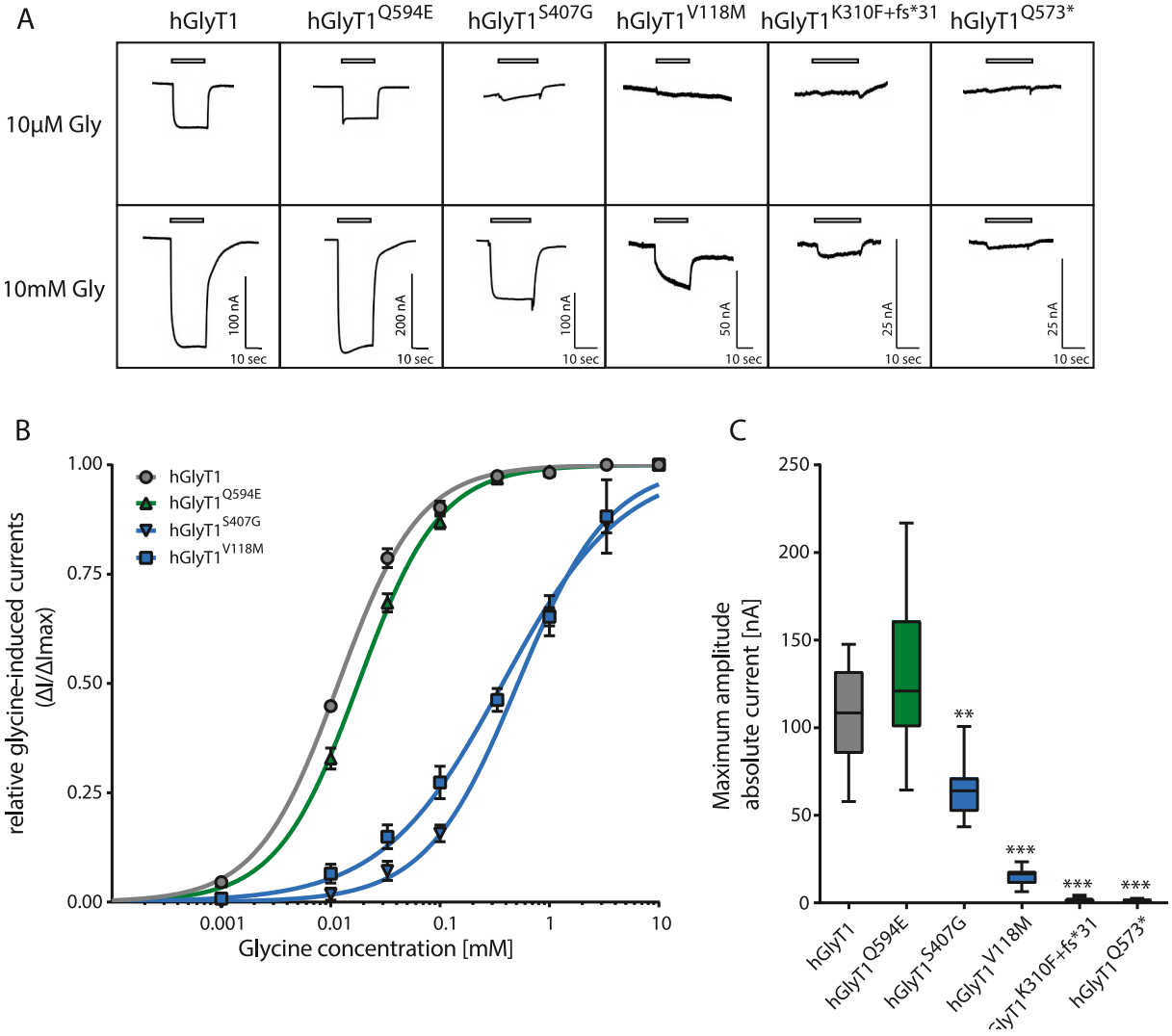


**Fig. 5.** Functional characterization of hGlyT1 mutations. (A) Original traces of electrophysiological measurements in *Xenopus leavis* oocytes expressing different hGlyT1 mutants compared to the wild type hGlyT1 after superfusion with 10 μM and 10 mM glycine, respectively. (B) Dose response curves for the respective hGlyT1 mutants showing the glycine induced currents in relation to the maximum observed current induced by 10 mM glycine. Of note, both truncated mutants showed no activity and were therefore omitted from the graph. (C) Maximum glycine induced current amplitudes determined on oocytes expressing the different hGlyT1 mutants (for all measurements n > 8, p < 0.01 (**), p < 0.001 (***), two way ANOVA with Bonferroni post hoc correction).

shorter polypeptide (Eulenburg et al., 2006). This was further confirmed by our surface biotinylation experiments, showing that both truncated transporters are excluded from the surface fraction at large. In line with these findings, injection of cRNAs encoding for neither of these transporter mutations produced glycine induced currents in *Xenopus laevis* oocytes, demonstrating that these transporters are completely deficient of glycine transport activity. This is concordant with previous findings demonstrating that amino acid residues essential for the COP II dependent ER exit (i.e. the $R^{575}L^{576}(X_8)D^{585}$ motive) are located in the carboxyl tail of the protein (Fernández-Sánchez et al., 2008) which is lacking in these mutant transporters.

In contrast to the truncated transporters hGlyT1$^{Q573*}$ and hGlyT1$^{K310F+fs*31}$, GlyT1 immunoreactive bands detected in Western blots from hGlyT1$^{S407G}$ and hGlyT1$^{V118M}$ were indistinguishable from those of wild-type hGlyT1 expressing cells, demonstrating that these proteins are expressed and carry most likely normal posttranslational modifications. This was verified by analysis of the glycosylation pattern of the transporter and wild-type-like stability in MD simulations. Furthermore, immunohistochemical as well as our surface biotinylation analysis demonstrated that both mutants reach the plasma membrane. Here, both mutants showed reduced signals in the pellet fraction containing the surface proteins. There was, however, no increase in the corresponding band in the flow through, containing the unlabelled cytosolic proteins, detectable. The most likely explanation for the discrepancy is loss of hGlyT1 protein e.g. due to an increase in transporter aggregation that are insoluble under the assay conditions used. Although this was only observed for both mutants but not for the wild-type hGlyT1 protein, this finding does not allow any conclusion on the stability of the mutant hGlyT1 proteins under physiological conditions. Furthermore it has to be noted, that, since these experiment were performed in HEK293 cells, additional differences on protein stability, e.g. in astrocytes i.e. the cell population showing highest GlyT1 expression *in-vivo*, cannot be excluded.

In line with a normal synthesis of the mutant transporter, glycine induced currents were readily detectable in oocytes expressing both transporter mutants, but only in the presence of very high glycine concentrations. Whereas wild-type hGlyT1 displays a Km of 11 μM, hGlyT1$^{S407G}$ showed a Km of 514 μM and the hGlyT1$^{V118M}$ mutant a Km of 373 μM. Also, the maximum inducible currents were strikingly reduced to approximately 60% for hGlyT1$^{S407G}$ and 20% for hGlyT1$^{V118M}$ of observed currents in wild-type hGlyT1 expressing oocytes, respectively. Although the reduced current amplitude might at least in part result from differences in cRNA quality used for injection, these data demonstrate that due to the reduced glycine affinity the respective mutations result in an almost entire loss of GlyT1 function under physiological conditions in both cases.

Structural models of GlyT1 on the basis of the crystal structure of the human serotonin and/or the bacterial LeuTa suggest that the Ser407 is localized within the transmembrane domain 7 and its hydroxyl-group is in very close proximity to both the ion binding sites for sodium and chloride (Coleman et al., 2016; Grouleff et al., 2015; Yamashita et al., 2005). This is also recapitulated in our structural model presented here. The strong functional impairment of the hGlyT1$^{S407G}$ mutant suggests that the hydroxyl group has important functions in ion binding directly and/or stabilization of the ion binding sites during conformational transition of the empty transporter. The MD simulations corroborate this hypothesis. They suggest, that the negative effect of S407G on glycine transport is likely transmitted via an impaired stabilization of the bound chloride ion that indirectly stabilizes Na1 in its binding site, whereas the mutation appears not to affect glycine binding, directly.

Sequence comparison to DAT and SERT suggest that Val118 is localized within the unwound part in the middle of TM1 that forms essential parts of both the ion and substrate binding site in transporters of the SLC6A family (Coleman et al., 2016; Grouleff et al., 2015; Wang et al., 2015; Yamashita et al., 2005). Interestingly, many interactions within this region of the transporter are not mediated by the amino acid side chains, but by the peptide backbone. Here the Carboxy-Oxygen of Val97 in SERT that is homologous to Val118 in hGlyT1 was shown to interact directly with the sodium bound to the second sodium binding site. An amino acid exchange to methionine at this position may result in a shift of positioning of this Carboxy group and thus might interfere with sodium binding (Coleman et al., 2019). MD simulations revealed, that V118M leads to a slight shift in the peptide backbone in the region of the mutation that results in a reduced hydrogen bonding and altered binding patterns for residues that stabilize the ligand amino group (i.e. contacts involving residues Tyr116 and Ser371). Although this does not lead to unbinding of the ligand in our simulations, it is tempting to speculate that the altered binding pattern at least contributes to the reduced glycine affinity observed in our functional assays.

In all GlyT1 encephalophathy patients, severe malformations like arthrogryposis and dysmorphic facial features have been observed. This contrasts mouse models carrying GlyT1 deficiencies, that showed only neurological abnormalities like respiratory depression or –for mice with neuronal GlyT1 deficiency– altered learning behaviour (Dubroqua et al., 2012; Eulenburg et al., 2010; Yee et al., 2006). Future studies will have to analyse the differences in GlyT1 functions between humans and rodents.

In summary, we could show that truncation of the transporter caused by the hGlyT1$^{Q573*}$ and hGlyT1$^{K310F+fs*31}$ mutations resulted in a complete loss of GlyT1 function. The transporter is not processed correctly and not translocated into the cell membrane, where it could facilitate glycine transport. The missense mutations hGlyT1$^{S407G}$ and hGlyT1$^{V118M}$ are processed correctly and inserted into the plasma membrane, but their transport activity is severely diminished and most likely constitutes a functional knock out under physiological conditions. Thus, our results support the hypothesis that the loss of GlyT1 function is causative for the symptoms seen in GlyT1 encephalopathy patients.

## 4. Materials and methods

### 4.1. Genetic analysis

The parents of the two fetuses received genetic counselling and agreed to the genomic analysis and the subsequent analysis of the identified mutation. For the genetic analysis DNA was extracted from cord blood of the fetus, and conducted whole exome sequencing on a NovaSeq6000 platform (Illumina, San Diego, USA) after enrichment with the SureSelectXT Human All Exon v6 kit (Agilent, Santa Clara, USA). Sequencing reads were mapped to the Genome Reference Consortium Human Genome Build 37 (GRCh37) using BWA-0.5.10,14. Duplicates were removed using samblaster,15. Single-nucleotide variants and small insertions/deletions were called using freebays 16 and annotated using SnpEff-3.3 (Ensembl-GRCh37.73),17. Sequencing data was analysed using the megSAP pipeline (https://github.com/imgag/megSAP). The variant list was filtered for rare variants (MAF $< 1\%$) with a potential effect on protein structure. Classification of the identified variants substantially followed ACMG guidelines (Richards et al., 2015). Segregation analysis was performed with Sanger sequencing using the BigDye Terminator v3.1 kit (Thermo Fisher Scientific, Waltham, USA) after amplification using FastSart Taq DNA polymerase (Sigma-Aldrich, St. Louis, USA) according to manufacturer's instructions.

### 4.2. Plasmids

Point mutations, hGlyT1$^{S407G}$, hGlyT1$^{Q594E}$ and hGlyT1$^{V118M}$, were inserted into a pcDNA3.1 plasmid carrying the hGlyT1 cDNA (R&D Systems) using the QuikChange Lightning and QuickChange XL Site-Directed Mutagenesis Kits (Agilent technologies, Santa Clara, USA). For the truncated mutations, hGlyT1$^{K310F+fs*31}$ and hGlyT1$^{Q573*}$, a Myc-tag was inserted after 13AA in frame in a two-step PCR based approach using Pfu DNA Polymerase (Promega, Madison, USA) into the hGlyT1-

pcDNA3.2 before using the QuikChange Lightning Site-Directed Mutagenesis Kit (Agilent technologies, Santa Clara, USA). All plasmids were verified by sequencing. Additionally, the pDsRed2-ER (Clontech, Mountain View, USA) and mGlyT2 (Armsen et al., 2007) plasmid was used for Immunocytochemistry.

### 4.3. Cell culture

HEK293 cells were cultured in DMEM with 10% fetal bovine serum, 1% Glutamine and 1% Penicillin-Streptomycin (Gibco, Thermo Fisher Scientific, USA) on 6 wells with a diameter of 34.8 mm for biotinylation and deglycosilation experiments or on glass coverslips with 12 mm (Wenzel, Germany) diameter coated with poly-L-lysine in 24 wells (Sarstedt, Nümbrecht, Deutschland) for immunocytochemistry. Cells were transfected with Lipofectamine 2000 (Thermo Scientific, USA) following manufacturers instructions for 24 h and cultured for further 24 h.

### 4.4. Western blotting

HEK293 cells were lysed 48 h after transfection in 2 mg/mL Dodecylmaltosid or 0.1% (v/v) NP40 in PBS (bioWORLD, USA) and protease inhibitor cocktail (Roche, Switzerland). Protein samples were diluted in 4x sample buffer (62.5 mM Tris-HCl pH 6.8, 2% SDS, 20% glycerol, 0,01% pyronin Y or bromphenolblue, 407.5 mM β-mercaptoethanol or 200 mM dithiothreitol) and analysed by SDS-PAGE and Western blotting as described (Eulenburg et al., 2006). Antibodies used are Rabbit anti-GlyT1 (Synaptic Systems, Germany) and Rabbit anti-Myc (Santa--Cruz, USA).

### 4.5. Deglycosylation

HEK 293 cells were lysed 48 h after transfection in 2 mg/mL Dodecylmaltosid or 0.1% (v/v) NP40 in PBS (bioPLUS Chemical, USAs) and protease inhibitor cocktail (Roche, Switzerland). Protein samples were treated with 500 U PNGaseF or EndoH (New England Biolabs, USA) for 90 min at 37 °C before stopping the reaction with sample buffer and proceeding to Western blot analysis.

### 4.6. Biotinylation

HEK 293 cells were washed with ice cold PBS (pH = 7,9) and treated with 2 mL of a 0.24 mg/mL EZ-Link™ Sulfo–NHS–SS-Biotin (Thermo Fisher Scientific, USA) for 40 min at 4 °C, quenched with 100 mM glycine in PBS, washed with PBS and lysed in 1% (v/v) NP40 (bioWORLD, USA) and protease inhibitor (Roche, Switzerland) (lysate fraction, L). 25 µg protein (0,5 µg/µL) was coupled to 50 µL PBS washed Streptavidin-agarose beads (Thermo Fisher Scientific, USA) for 3 h at 4 C while overhead shaking. The beads were pelleted (1000×*g*, 3 min), the intracellular fraction collected (flow through fraction, F) and after washing with PBS (wash fraction, W) the proteins were eluted (pellet fraction, P) from the beads using an equivalent volume 2x sample buffer containing 50 mM DTT for 30 min at 37 °C. The collected samples were then analysed by Western blot.

### 4.7. Immunocytochemistry

After washing with PBS, transfected HEK293 cells were fixed in 4% paraformaldehyde in PBS for 10 min on ice, quenched with 100 mM glycine in PBS and blocked and permeabilized for 30 min in blocking solution (2% (w/v) bovine serum albumin, 2% (v/v) normal goat serum and 0.3% (v/v) Triton-X-100 in PBS). The cells were then incubated with primary antibody diluted in blocking solution for 2 h at room temperature in a wet chamber, washed with PBS and incubated with secondary antibody (Alexa 488 and Alexa 635 conjugated goat antibodies raised against the respective species, Thermo Fisher, USA) and in blocking solution for 1h at room temperature in a wet chamber, followed by incubation with DAPI in PBS for 10 min at room temperature. After washing in PBS, the glass coverslips were briefly dipped in water and mounted on microscopy slides using Aqua Polymount (Polyscience Inc., USA). Antibodies used are rabbit GlyT1 (Synaptic Systems, Germany) of for colabeling experimentsguinea pig anti-GlyT1 (Schlösser et al., 2015) and rabbit anti-Myc (Abcam, USA). HEK 293 cells were imaged using a 63 x objective on an LSM800 laser scanning microscope (Zeiss, Germany). Mander's coefficients, as indicators for colocalization were calculated using ImageJ (Bolte and Cordelières, 2006; Schindelin et al., 2012).

### 4.8. Molecular dynamics simulation

Molecular dynamics simulations used a previously generated homology model of hGlyT1 based on LeuTa (Bartholomäus et al., 2008). Point mutations were introduced with The PyMOL Molecular Graphics System, (Version 2.0 Schrödinger, LLC). The protein was embedded into a solvated 1-palmitoyl-2-oleoyl-sn-glycero-3-phosphocholine (POPC) bilayer using CHARMM-GUI (Wu et al., 2014). The solvent ion concentration was 0.15 mol/l NaCl. Prior to simulation, we placed 2 sodium ions (Na1, Na2), 1 chloride and a zwitterionic glycine inside the channel at their suggested binding sites (Alfadhel et al., 2016; Fratev et al., 2019).

Simulations were carried out with GROMACS 2020 (Abraham et al., 2015; Van Der Spoel et al., 2005) in combination with the Amber99SB*-ILDN force field (Best and Hummer, 2009; Lindorff-Larsen et al., 2010), the TIP3P water model (Jorgensen et al., 1983), Berger-derived POPC lipids (Cordomí et al., 2012) and ion parameters by Joung and Cheatham (2008). Zwitterionic glycine parameters were taken from Horn (2014). Van-der-Waals interactions were cut-off at 1 nm and electrostatics were treated by PME (Essmann et al., 1995) beyond 1 nm. Temperature and Pressure were kept at 310 K and 1 bar using the stochastic V-Rescale Thermostat (Bussi et al., 2007) and Parrinello-Rahman Barostat (Parrinello and Rahman, 1981), respectively. Bonds involving hydrogen atoms were kept constant using LINCS (Hess et al., 1997). The time step was 2 fs. After system preparation, we performed 2000 steps energy minimization (steepest descent) and 20 ns position-restrained equilibration (Fc = 1000 kJ/mol/nm2). Finally, restraints were gradually lifted over 3 ns, followed by 250ns unrestrained simulation. Molecular dynamics trajectories were analysed using GROMACS tools and Biotite (Kunzmann and Hamacher, 2018). The Baker-Hubbard algorithm (Baker and Hubbard, 1984) was used to detect hydrogen bonds and polar contacts involving ions were calculated by a distance criterion of 0.3 nm.

### 4.9. Electrophysiology

Defolliculated *Xenopus laevis* oocytes were purchased from EcoCyte Bioscience Germany. The oocytes were injected with 46 nl of cRNA (1 µg/µl), stored in ND96 solution (in mM NaCl 960; KCl 20; $CaCl_2$ 10; $MgCl_2$ 10; HEPES 50; pH 7.4) and incubated for 4 days at 16 °C. Oocytes were superfused with ND96 solution without calcium containing different concentrations of glycine. Currents mediated by recombinant expressed glycine transporters were determined using the two-electrode-voltage-clamp (TEVC) technique. Substance induced currents were measured as changes of the stable baseline during solution change at a set membrane potential of – 50 mV. Current traces were recorded after amplification by a TurboTec-03X (npi elctronics, Germany) and analysed using the software Cell Works and Cell Works Reader (npi electronics, Germany).

## Author's contributions

Katharina Hauf: Investigation, methodology, formal analysis, writing-original draft, visualization; Lukas Barsch, Investigation, formal

analysis; Daniel Bauer: Investigation, formal analysis; Rebecca Buchert: Investigation; Anja Armbruster: Investigation; Leonie Frauenfeld: Investigation; Ute Grasshoff: Investigation; Volker Eulenburg: Conceptualization, Investigation, Supervision, Project administration, writing -original draft. All authors have read and approved the final draft of the manuscript.

## Declaration of competing interest

The authors have nothing to declare.

## Acknowledgements

We would like to thank Ina Bosse and Konstanze Büttner, for excellent technical assistance. This work was supported by fundings from the Leipzig University and a Grant from the Deutsche Forschungs Gemeinschaft to V.E. (DFG, EU110/6-1). Calculations for this research were conducted on the Lichtenberg high performance computer of the TU Darmstadt.

## References

Abraham, M.J., Murtola, T., Schulz, R., Páll, S., Smith, J.C., Hess, B., Lindahl, E., 2015. GROMACS: high performance molecular simulations through multi-level parallelism from laptops to supercomputers. SoftwareX 1–2, 19–25. https://doi.org/10.1016/j.softx.2015.06.001.

Alfadhel, M., Nashabat, M., Qahtani, H.A., Alfares, A., Mutairi, F.A., Shaalan, H.A., Douglas, G.V., Wierenga, K., Juusola, J., Alrifai, M.T., Arold, S.T., Alkuraya, F., Ali, Q.A., 2016. Mutation in SLC6A9 encoding a glycine transporter causes a novel form of non-ketotic hyperglycinemia in humans. Hum. Genet. 135, 1263–1268. https://doi.org/10.1007/s00439-016-1719-x.

Alfallaj, R., Alfadhel, M., 2019. Glycine transporter 1 encephalopathy from biochemical pathway to clinical disease: review. Child Neurol. Open 6. https://doi.org/10.1177/2329048X19831486, 2329048X1983148.

Applegarth, D.A., Toone, J.R., 2001. Nonketotic hyperglycinemia (Glycine encephalopathy): laboratory diagnosis. Mol. Genet. Metabol. 74, 139–146. https://doi.org/10.1006/mgme.2001.3224.

Armsen, W., Himmel, B., Betz, H., Eulenburg, V., 2007. The C-terminal PDZ-ligand motif of the neuronal glycine transporter GlyT2 is required for efficient synaptic localization. Mol. Cell. Neurosci. 36, 369–380. https://doi.org/10.1016/j.mcn.2007.07.011.

Baker, E.N., Hubbard, R.E., 1984. Hydrogen bonding in globular proteins. Prog. Biophys. Mol. Biol. 44, 97–179. https://doi.org/10.1016/0079-6107(84)90007-5.

Bartholomäus, I., Laura, M.-L., Nicke, A., Dutertre, S., Hastrup, H., Jha, A., Gether, U., Sitte, H.H., Betz, H., Eulenburg, V., 2008. Glycine transporter dimers: evidence for occurrence in the plasma membrane. J. Biol. Chem. 283, 10978–10991. https://doi.org/10.1074/jbc.M800622200.

Best, R.B., Hummer, G., 2009. Optimized molecular dynamics force fields applied to the Helix−Coil transition of polypeptides. J. Phys. Chem. B 113, 9004–9015. https://doi.org/10.1021/jp901540t.

Bolte, S., Cordelières, F.P., 2006. A guided tour into subcellular colocalization analysis in light microscopy. J. Microsc. 224, 213–232. https://doi.org/10.1111/j.1365-2818.2006.01706.x.

Bussi, G., Donadio, D., Parrinello, M., 2007. Canonical sampling through velocity rescaling. J. Chem. Phys. 126, 014101 https://doi.org/10.1063/1.2408420.

Coleman, J.A., Green, E.M., Gouaux, E., 2016. X-ray structures and mechanism of the human serotonin transporter. Nature 532, 334–339. https://doi.org/10.1038/nature17629.

Coleman, J.A., Yang, D., Zhao, Z., Wen, P.-C., Yoshioka, C., Tajkhorshid, E., Gouaux, E., 2019. Serotonin transporter-ibogaine complexes illuminate mechanisms of inhibition and transport. Nature 569, 141–145. https://doi.org/10.1038/s41586-019-1135-1.

Cordomí, A., Caltabiano, G., Pardo, L., 2012. Membrane protein simulations using AMBER force field and berger lipid parameters. J. Chem. Theor. Comput. 8, 948–958. https://doi.org/10.1021/ct200491c.

Dubroqua, S., Serrano, L., Boison, D., Feldon, J., Gargiulo, P.A., Yee, B.K., 2012. Intact working memory in the absence of forebrain neuronal glycine transporter 1. Behav. Brain Res. 230, 208–214. https://doi.org/10.1016/j.bbr.2012.01.061.

Essmann, U., Perera, L., Berkowitz, M.L., Darden, T., Lee, H., Pedersen, L.G., 1995. A smooth particle mesh Ewald method. J. Chem. Phys. 103, 8577–8593. https://doi.org/10.1063/1.470117.

Eulenburg, V., Becker, K., Gomeza, J., Schmitt, B., Becker, C.-M.M., Betz, H., 2006. Mutations within the human GLYT2 (SLC6A5) gene associated with hyperekplexia. Biochem. Biophys. Res. Commun. 348, 400–405. https://doi.org/10.1016/j.bbrc.2006.07.080.

Eulenburg, V., Retiounskaia, M., Papadopoulos, T., Gomeza, J., Betz, H., 2010. Glial glycine transporter 1 function is essential for early postnatal survival but dispensable in adult mice. Glia 58, 1066–1073. https://doi.org/10.1002/glia.20987.

Fernández-Sánchez, E., Díez-Guerra, F.J., Cubelos, B., Giménez, C., Zafra, F., 2008. Mechanisms of endoplasmic-reticulum export of glycine transporter-1 (GLYT1). Biochem. J. 409, 669–681. https://doi.org/10.1042/BJ20070533.

Fratev, F., Miranda-Arango, M., Lopez, A.B., Padilla, E., Sirimulla, S., 2019. Discovery of GlyT2 inhibitors using structure-based pharmacophore screening and selectivity studies by FEP+ calculations. ACS Med. Chem. Lett. 10, 904–910. https://doi.org/10.1021/acsmedchemlett.9b00003.

Gomeza, J., Armsen, W., Betz, H., Eulenburg, V., 2006. Lessons from the knocked-out Glycine transporters. In: Sitte, H.H., Freissmuth, M. (Eds.), Neurotransmitter Transporters. Springer-Verlag, Berlin/Heidelberg, pp. 457–483. https://doi.org/10.1007/3-540-29784-7_19.

Gomeza, J., Hulsmann, S., Ohno, K., Eulenburg, V., Szoke, K., Richter, D., Betz, H., 2003a. Inactivation of the glycine transporter 1 gene discloses vital role of glial glycine uptake in glycinergic inhibition. Neuron 40, 785–796.

Gomeza, J., Ohno, K., Hulsmann, S., Armsen, W., Eulenburg, V., Richter, D.W., Laube, B., Betz, H., 2003b. Deletion of the mouse glycine transporter 2 results in a hyperekplexia phenotype and postnatal lethality. Neuron 40, 797–806.

Grouleff, J., Ladefoged, L.K., Koldsø, H., Schiøtt, B., 2015. Monoamine transporters: insights from molecular dynamics simulations. Front. Pharmacol. 6 https://doi.org/10.3389/fphar.2015.00235.

Hess, B., Bekker, H., Berendsen, H.J.C., Fraaije, J.G.E.M., 1997. LINCS: a linear constraint solver for molecular simulations. J. Comput. Chem. 18, 1463–1472. https://doi.org/10.1002/(SICI)1096-987X(199709)18:12<1463::AID-JCC4>3.0.CO;2-H.

Horn, A.H.C., 2014. A consistent force field parameter set for zwitterionic amino acid residues. J. Mol. Model. 20, 2478. https://doi.org/10.1007/s00894-014-2478-z.

Jorgensen, W.L., Chandrasekhar, J., Madura, J.D., Impey, R.W., Klein, M.L., 1983. Comparison of simple potential functions for simulating liquid water. J. Chem. Phys. 79, 926–935. https://doi.org/10.1063/1.445869.

Joung, I.S., Cheatham, T.E., 2008. Determination of alkali and halide monovalent ion parameters for use in explicitly solvated biomolecular simulations. J. Phys. Chem. B 112, 9020–9041. https://doi.org/10.1021/jp8001614.

Kunzmann, P., Hamacher, K., 2018. Biotite: a unifying open source computational biology framework in Python. BMC Bioinf. 19, 346. https://doi.org/10.1186/s12859-018-2367-z.

Kurolap, A., Armbruster, A., Hershkovitz, T., Hauf, K., Mory, A., Paperna, T., Hannappel, E., Tal, G., Nijem, Y., Sella, E., Mahajnah, M., Ilivitzki, A., Hershkovitz, D., Ekhilevitch, N., Mandel, H., Eulenburg, V., Baris, H.N., 2016. Loss of Glycine transporter 1 causes a subtype of Glycine encephalopathy with arthrogryposis and mildly elevated cerebrospinal fluid Glycine. Am. J. Hum. Genet. 99, 1172–1180. https://doi.org/10.1016/j.ajhg.2016.09.004.

Lindorff-Larsen, K., Piana, S., Palmo, K., Maragakis, P., Klepeis, J.L., Dror, R.O., Shaw, D. E., 2010. Improved side-chain torsion potentials for the Amber ff99SB protein force field. Proteins Struct. Funct. Bioinf. 78, 1950–1958. https://doi.org/10.1002/prot.22711.

Lynch, J.W., 2004. Molecular structure and function of the Glycine receptor chloride channel. Physiol. Rev. 84, 1051–1095. https://doi.org/10.1152/physrev.00042.2003.

Martina, M., Gorfinkel, Y., Halman, S., Lowe, J.A., Periyalwar, P., Schmidt, C.J., Bergeron, R., 2004. Glycine transporter type 1 blockade changes NMDA receptor-mediated responses and LTP in hippocampal CA1 pyramidal cells by altering extracellular glycine levels: blockade of GlyT1 changes LTP. J. Physiol. 557, 489–500. https://doi.org/10.1113/jphysiol.2004.063321.

Martina, M., Marie-Eve, B.-T., Halman, S., Tsai, G., Tiberi, M., Coyle, J.T., Bergeron, R., 2005. Reduced glycine Transporter Type 1 Expression Leads to Major Changes in Glutamatergic Neurotransmission of CA1 Hippocampal Neurones in Mice, vol. 563, pp. 777–793. https://doi.org/10.1113/jphysiol.2004.080655.

Martínez-Maza, R., Poyatos, I., López-Corcuera, B., N úñez, E., Giménez, C., Zafra, F., Aragón, C., 2001. The role of N-glycosylation in transport to the plasma membrane and sorting of the neuronal glycine transporter GLYT2. J. Biol. Chem. 276, 2168–2173. https://doi.org/10.1074/jbc.M006774200.

Parrinello, M., Rahman, A., 1981. Polymorphic transitions in single crystals: a new molecular dynamics method. J. Appl. Phys. 52, 7182–7190. https://doi.org/10.1063/1.328693.

Richards, S., Aziz, N., Bale, S., Bick, D., Das, S., Gastier-Foster, J., Grody, W.W., Hegde, M., Lyon, E., Spector, E., Voelkerding, K., Rehm, H.L., ACMG Laboratory Quality Assurance Committee, 2015. Standards and guidelines for the interpretation of sequence variants: a joint consensus recommendation of the American college of medical genetics and genomics and the association for molecular pathology. Genet. Med. Off. J. Am. Coll. Med. Genet. 17, 405–424. https://doi.org/10.1038/gim.2015.30.

Schindelin, J., Arganda-Carreras, I., Frise, E., Kaynig, V., Longair, M., Pietzsch, T., Preibisch, S., Rueden, C., Saalfeld, S., Schmid, B., Tinevez, J.-Y., White, D.J., Hartenstein, V., Eliceiri, K., Tomancak, P., Cardona, A., 2012. Fiji: an open-source platform for biological-image analysis. Nat. Methods 9, 676–682. https://doi.org/10.1038/nmeth.2019.

Schlösser, Lukas, Barthel, Franziska, Brandenburger, Timo, Neumann, Elena, Bauer, Inge, Eulenburg, Volker, Werdehausen, Robert, Hermanns, Henning, 2015. Glycine transporter GlyT1, but not GlyT2, is expressed in rat dorsal root ganglion—Possible implications for neuropathic pain. Neurscience Letters 600, 213–219. https://doi.org/10.1016/j.neulet.2015.06.026.

Sievers, F., Wilm, A., Dineen, D., Gibson, T.J., Karplus, K., Li, W., Lopez, R., McWilliam, H., Remmert, M., Söding, J., Thompson, J.D., Higgins, D.G., 2011. Fast, scalable generation of high-quality protein multiple sequence alignments using Clustal Omega. Mol. Syst. Biol. 7, 539. https://doi.org/10.1038/msb.2011.75.

Van Der Spoel, D., Lindahl, E., Hess, B., Groenhof, G., Mark, A.E., Berendsen, H.J.C., 2005. GROMACS: fast, flexible, and free. J. Comput. Chem. 26, 1701–1718. https://doi.org/10.1002/jcc.20291.

Wang, K.H., Penmatsa, A., Gouaux, E., 2015. Neurotransmitter and psychostimulant recognition by the dopamine transporter. Nature 521, 322–327. https://doi.org/10.1038/nature14431.

Wu, E.L., Cheng, X., Jo, S., Rui, H., Song, K.C., Dávila-Contreras, E.M., Qi, Y., Lee, J., Monje-Galvan, V., Venable, R.M., Klauda, J.B., Im, W., 2014. CHARMM-GUI Membrane Builder toward realistic biological membrane simulations. J. Comput. Chem. 35, 1997–2004. https://doi.org/10.1002/jcc.23702.

Yamashita, A., Singh, S.K., Kawate, T., Jin, Y., Gouaux, E., 2005. Crystal structure of a bacterial homologue of Na+/Cl–dependent neurotransmitter transporters. Nature 437, 215–223. https://doi.org/10.1038/nature03978.

Yee, B.K., Balic, E., Singer, P., Schwerdel, C., Grampp, T., Gabernet, L., Knuesel, I., Benke, D., Feldon, J., Mohler, H., Boison, D., 2006. Disruption of Glycine transporter 1 restricted to forebrain neurons is associated with a procognitive and antipsychotic phenotypic profile. J. Neurosci. 26, 3169–3181. https://doi.org/10.1523/JNEUROSCI.5120-05.2006.

Zafra, F., Aragón, C., Olivares, L., Danbolt, N., Giménez, C., J, S.-M., 1995. Glycine transporters are differentially expressed among CNS cells. J. Neurosci. 15, 3952–3969.